Heme-induced ferroptosis promotes human lumbar disc degeneration analyzed by MALDI-TOF MS

Liang Shan
Shanghai University of TCM: Shanghai University of Traditional Chinese Medicine
Ximing Xu
The Second Military Medical University
Jing Zhang (zhangjing@sioc.ac.cn)
Shanghai Institute of Organic Chemistry
Peng Cai
Shanghai Institutes of Nutrition and Health CAS: Chinese Academy of Sciences Shanghai Institutes of Nutrition and Health
Han Gao
Shanghai University of TCM: Shanghai University of Traditional Chinese Medicine
Yingjie Lu
Shanghai University of Traditional Chinese Medicine
Jiangang Shi (shijiangang616@163.com)
The Second Military Medical University
Yinlong Guo
Shanghai Institute of Organic Chemistry
Yue Su (suyue@shutcm.edu.cn)
Shanghai University of Traditional Chinese Medicine https://orcid.org/0000-0002-4388-7452

Research article

Keywords: disc degeneration, heme-iron, ferropotosis, vasculogenesis, MALDI-TOF MS, biomarker

DOI: https://doi.org/10.21203/rs.3.rs-361502/v1

Abstract

Background

Neovasculogenesis is a characteristic of degenerative lumbar discs, which makes extruded tissues exposed to heme-iron cytotoxicity (increased oxidative stress by ferroptosis). However, the present analyses for neovascularization are very complicated, and its mechanism of action is rarely reported.

Methods

Matrix-assisted laser desorption/ionization time-of-flight mass spectrometry (MALDI-TOF MS) was performed to analyze human degenerative lumbar discs. Then, clinical relevance was analyzed between MALDI-TOF MS results and Pfirrmann classification of degenerative discs. In order to explore the mechanism, a heme-induced ferroptosis effect was evaluated both at tissue and cell levels using high-resolution MALDI-TOF MS and molecular biology methods.

Results

The spectra revealed that hemoglobin (Hb) and heme signals were highly increased, thus serving as biomarkers of vasculogenesis in degenerative tissues. Clinical relevance analysis demonstrated that the intensity of Hb and heme peaks was closely related to Pfirrmann classification of degenerative discs. Mechanically, increased heme catabolism and down-regulation of glutathione peroxidase 4 (GPX4) levels were detected in degenerative discs, reflecting a iron-dependent cell death or ferroptosis. Further, accuracy mass measurements confirmed that the levels of ferroptosis-related metabolites such as glutathione, arachidonic acid (AA), sphinganine, polyunsaturated fatty acid (PUFA), and tricarboxylic acid (TCA) cycle were significantly different between the degenerative and normal tissues, indicating the interior of degenerative tissues was a prooxidant environment. Moreover, the heme-induced ferroptosis was verified in human nucleus pulposus cells, and the underlying mechanism might be associated with the Notch pathway.

Conclusions

The neovascularization in degenerative discs may expose the tissues to high heme toxicity, which further induces the ferroptosis effect within the tissues and accelerates the degeneration progression of discs. This study is beneficial for the pathological mechanism in degenerative discs and facilitate the development of non-operative intervention for lumbar disc herniation (LDH).

Introduction

Lumbar disc herniation (LDH) is a common cause of chronic low back pain, with a lifetime prevalence of 84%, of which 11% of patients suffer serious disability due to LDH (Yao et al. 2020). Disc degeneration is a primary reason of LDH which is influenced by many factors including: age, histological structure, biomechanics, genes, inflammation, and osteoporosis (Qiu et al. 2020; Doraisamy et al. 2002; Petra et al.

2020). In 1993, neovascularization was first observed in degenerative discs of LDH patients by histological staining, and this phenomenon was closely related to age and disease duration (Yasuma et al. 1993). Vasculogenesis may be a repair process after disc injury, and also has a role in promoting tissue degradation (Xiao et al. 2020). But, the mechanism of vasculogenesis in disc degeneration still kept unclear.

A histological feature of impaired discs is the formation of vascularized granulation tissues from the nucleus pulposus to the annulus fibrosus along pathological tears of extruded tissues (Arai et al. 2000). In immature neovascularization, Hemoglobin (Hb) is liberated from extravasated red blood cells (RBCs). Then, the oxidation of Hb to ferrylhemoglobin (ferrylHb) resulted in the release of heme moieties (ferriporphyrin), a major source of intracellular iron (Nagy et al. 2010). Heme-iron constitutes the prosthetic group for proteins that influences many fundamental biological processes, including catalyzing free radical reactions within cells, signal transduction, respiration, and energetic homeostasis (Jeney et al. 2002; Hower et al. 2009; Yin et al. 2007). The aberrant accumulation of bio-iron will lead to nonapoptotic cell death caused by iron-dependent oxidative damage (ferroptosis), which is mainly characterized by reduced cell volume and increased mitochondrial membrane density (Dixon et al. 2012). Heme-induced ferroptosis is related to many acute traumas and chronic degenerative lesions, such as atherosclerotic process (Nagy et al. 2010), malignant tumors (Buss et al. 2004), and neurodegenerative disease (Zhang et al. 2020).

We considered that vascularized granulation tissues in degenerative discs were similar to hemorrhaged atherosclerotic plaques, thus neovasculogenesis must be implicated in many pathological changes of LDH. However, the current analysis was still lacked for neovasculogenesis in degenerative discs. Unlike tumor tissues with abundant vessels, it was difficult to obtain the vascularized zone during sectioning in newly-vascularized granulation tissues in discs, which greatly affected the reliability of results. Additionally, in the progression of disc degeneration, a decrease in nucleus pulposus water was concomitant with the degeneration of proteoglycan and collagen, causing discs to shrink and become floppy (Arai et al. 2000). Hence it was a challenge to obtain structured histology sections in practice.

Matrix-assisted laser desorption/ionization time-of-flight mass spectrometry (MALDI-TOF MS) has advantages of lower-cost and automation, and has made considerable advances in the research of cancer, cardiovascular diseases, and infectious diseases (Wang et al. 2011; Wieczorek et al. 2020; van Smaalen et al. 2019). The direct analysis of body fluids or tissue samples using MALDI-TOF MS can identify specific biomarkers and further reveal the characteristic pathological changes of diseases (Grand et al. 2014).

In this study, MALDI-TOF MS was used to directly analyze degenerative discs and normal control discs aiming to find differentially expressed molecules that could rapidly and accurately assess vasculogenesis. Importantly, a heme-induced ferroptosis mechanism was firstly proven to involved in disc degeneration both at tissue and cell levels.

Materials And Methods

Patients and tissue samples

All patients accepted informed consent before enrollment. The study was conducted in accordance with the Declaration of Helsinki, and the protocol was approved by the Medical Ethics Committee, Shanghai Changzheng Hospital. Clinicopathological characteristics of patients were shown in Table 1.

Table 1
Clinicopathological characteristics of LDH patients and control patients with tethered cord syndrome.

No.	Sample	Gender	Ages	Pfirrmann	Segment
1	475	female	18	TCS	L4/L5
2	854	male	18	TCS	L4/L5
3	877	male	28	TCS	L3/L4
4	560	female	36	TCS	L4/L5
5	407	female	18	TCS	L1/L2
6	382	female	18	TCS	L2/L3
7	975	female	18	TCS	L3/L4
8	884	male	19	TCS	L2/L3
9	004	male	19	TCS	L3/L4
10	961	female	51	4	L4/L3
11	532	male	40	3	L4/L5
12	570	male	22	3/4	L4/L5
13	973	female	28	4	L4/L5
14	988	male	62	4	L4/L5
15	017	male	63	4	L3/L4
16	404	male	63	3	L3/L4
17	090	female	67	3/4	L5/S1
18	535	male	37	3	L3/L4
19	557	male	64	4/5	L3/L4
20	602	male	56	4/5	L4/L5
21	039	male	55	4	L4/L5
22	045	female	67	4	L4/L5
23	019	female	47	4	L4/L5
24	100	female	54	4/5	L2/L3
25	001	female	54	3	L4/L5

Cell culture

The human primary nucleus pulposus cells (HNPCs) were provided by Shanghai YCBIO Co., Ltd. Cells were cultured in DMEM with 10 % fetal bovine serum and 1 % penicillin-streptomycin at a 37 ℃ cell culture incubator with 5 % CO_2. Hb (Sigma, H7379), heme (Sigma, 51281), deferoxamine mesylate salt (DFO) (Shycbio, Y1310), and ferric ammonium citrate (FAC) (Sigma, F5879) were dissolved with DMEM to a final concentration of 20 mg/mL. Feroptosis inducer erastin (Sigma, E7781) was dissolved with DMSO to a final concentration of 1 mg/mL. Storing at 4℃ for short-term use.

Protein extraction

After thawing, tissues were washed twice in deionized water to remove blood contamination on the surface. Then, samples were minced with scissors on ice and homogenized in RIPA buffer (Solarbio, R0010) containing 1 % phenylmethylsulfonyl fluoride (PMSF) at a ratio of 10 μL/mg. After that, homogenates were lysed at 4 ℃ for 30 min, then, centrifuged at 12000 g for 30 min at 4 ℃. For cell protein extraction, cells were lysed after treating with a series concentration of regentsextra for 24 h, then, centrifuged at 12000 g for 30 min at 4 ℃. Supernatants were collected as protein samples and stored at -80 ℃ until use.

MALDI-TOF MS analysis

The matrix was dissolved with a 1:1 mixture of acetonitrile and water (0.1 % trifluoroacetic acid) to a final concentration of 10 mg/mL. Sinapic acid was used as the matrix for Hb analysis, and dihydroxybenzoic acid was used as the matrix for heme analysis. Before MALDI-TOF MS analysis, 1.5 μL of mixture containing protein samples and matrix solution (1:40) was spotted on a MALDI plate and dried at room temperature. For Hb analysis, the spectra were collected using an Shimadzu biotech lauchpad MALDI-TOF MS (Shimadzu, Japan) equipped with a high-mass detector (CovalX AG, Switzerland) in Linear-CovalX mode. For heme analysis, the spectra were collected using an Shimadzu biotech lauchpad MALDI-TOF MS (Shimadzu, Japan) in Reflectron mode. Ionization was achieved using a N2 laser (337 nm) and 100 laser shots for each mass spectrum. The spectra were calibrated using external standards.

Accuracy mass of metabolites (m/z = 50-1000) were analyzed by MALDI Spiral TOF-TOF MS (JEOL, Japan) in Spiral mode. Ionization was achieved using a Nd:YLF laser (349 nm) and 2000 laser shots for each mass spectrum. Then, Human Metabolome Database (HMDB) (http://www.hmdb.ca/) were used to further identify potential biomarkers.

Western blotting analysis

Protein concentrations were tested by BCA Protein Assay Kit (Beyotime, P0012i). 20–30 μg of total protein was separated by 10 % SDS-PAGE (EpiZyme, pg112) and then transferred onto nitrocellulose membrane (Pall, 66485). Non-specific sites were blocked with 5 % non-fat milk in phosphate buffer saline (0.1 % Tween-20) at room temperature. Next, blots were incubated overnight at 4 ℃ with primary antibodies which were listed as follows: anti-Hb α (Santa Cruz, sc-514378), anti-Hb β (Santa Cruz, sc-

21757), anti-CD31 (Affinity, AF6191), anti-Glutathione Peroxidase 4 (GPX4) (Affinity, DF6701), anti-Heme Oxygenase-1 (HO-1) (Affinity, AF5393), anti-Bcl2 (ImmunoWay, YM3041), anti-Bax (ImmunoWay, YT0455), anti-Notch1 (Cell Signaling Technology, #3608), anti-Jag1 (Cell Signaling Technology, #70109), anti-Hes1 (Abcam, ab108937), anti-Hey1 (Abcam, ab154077), and anti-β-actin (Affinity, AF7018). The next day, blots were incubated by horseradish peroxidase (HRP) conjugated secondary antibodies (Affinity, s0001) and visualized by New Super ECL Assay (KeyGen BioTECH, KGP1128).

Cell viability analysis

10000 cells were inoculated in 96-well plates and treated for 24 h. After that, the old medium was replaced with 10 μl CCK-8 (Dojindo, CK04) and 100 μl DMEM, and then cells were incubated for 1 h at 37 ℃. The optical density (OD) at 450 nm was read using a microplate reader.

Immunohistochemistry (IHC)

Disc tissues were embedded in paraffin blocks and then cut into 7 μm sections. For IHC, One-Step IHC Assay (KeyGen, KGOS60) were used to stain 7μm thickness, and the paraffin sections were incubated with anti-GPX4 (Affinity, DF6701) and HO-1 (Affinity, AF5393).

qRT- PCR

Total RNA was extracted using TRIzol Reagent, and cDNA was synthetized with a RevertAidTM First Strand cDNA Synthesis Kit (Fermentas, Vilnius), then, qPCR was performed using The PCR Amplification Kit (Takara, R011). The specific primers are listed in Table 2.

Table 2
Primers used for qRT-PCR.

Name	Sequences (5'-3')
GAPDH-F	AACAGCCTCAAGATCATC
GAPDH-R	ACTGTGCAACCGTCACCC
Notch1-F	CAAAGTGTCTGAGGCCAG
Notch1-R	GTGAGTAAGACCAACAGC
Notch2-F	CTGCATGAACCATGGTCT
Notch2-R	ACCGTTCCTAACCGTTCC
Jag1-F	CAAGTGCACCCGCGACGA
Jag1-R	CCGTCGTGCTACGCCAAC
Jag2-F	CGCTGCGGAACGTGAACG
Jag2-R	GGAACCGGACCATGAGGA
Hes1-F	CGGCTGCGCTGAGCACAG
Hes1-R	CGCGCTTGCCGCGCACGA
Hes2-F	CTGCCTGGTCACTGCTCT
Hes2-R	CGGATCCTCACCTCCACT
Hey1-F	AGCAAGGATCTGCTAAGC
Hey1-R	GCATCAACAACTCTACGC

Statistical analysis

Comparisons between two populations were performed using two independent sample t-test. Differences between treatment group and control group were analyzed with student's t-test. Principal component analysis (PCA) and receiver operating curve (ROC) were performed on the MALDI-TOF MS data using the SPSS 21.0 (SPSS Inc., USA). P value less than 0.05 was considered statistically significant.

Results

Hb signals were highly increased in degenerative discs compared to normal discs

First tissue lysates from degenerative discs were analyzed by MALDI-TOF MS combined with a high-mass detector. As shown in Fig. 1a, some high intensity peaks were observed in the high-mass range (10–100 kDa). Through further analyzing the spectra of Hb standard, tissue lysates, and their mixture, these peaks were finally identified as Hb-related peaks. The protein peaks with m/z value of 16300 and 17100 were from Hb α and Hb β respectively, which were subunits of Hb (Fig. 1b). Then, we observed that Hb-related peaks clearly illustrated different intensity in the two kinds of tissues (Fig. 1c).

Normal discs are avascular tissues, while the variability of Hb contents in various tissues is one of indicators to assess vasculogenesis (Orellano et al. 2020). For this reason, high abundances of Hb may be of major value in the diagnosis of vasculogenesis in degenerative discs. To verify this, 13 cases of degenerative discs and 9 cases of normal disc tissues were further analyzed by MALDI-TOF MS combined with the high-mass detector. Figure 1d showed that Hb-related peaks with m/z value of 16300, 16500, 16700, 17100, and 17300 were differentially up-regulated in degenerative and normal discs ($P < 0.01$), except the protein peak with m/z value of 17700, suggesting high abundances of Hb were specific pattern in degenerative discs. Next, the high dimensional mass spectrometry (MS) date were processed using PCA. The first (83.2 %) and the second (13.4 %) principal components were chosen for visualization. As shown in Fig. 1e, clear separation of degenerative discs and normal control discs was obtained. The data classified into normal and diseased groups exhibited variations, indicating the heterogeneity between these two groups. In order to further explore the diagnostic value of various Hb-related peaks in degenerative discs, we used the ROC for analyzing MS data. As expected, the ROC analysis revealed positive ability of the 5 protein peaks to predict vasculogenesis in degenerative discs (Fig. 1f). In conclusion, these results demonstrated that Hb might be a candidate marker for vasculogenesis in degenerative discs.

Specific increase of heme contents in degenerative discs

In practice of clinical diagnosis, the analysis of large proteins is much more complicated than that of small molecule compounds. In this study, a commercial high-mass detector was incorporated with MALDI-TOF MS to detect intact high abundance proteins in human discs, although it had the advantages of celerity and accuracy, the cost was quite high. Accounting for this, the detection range of MS was extended to the low-mass range (100–2000 Da) in order to screen small markers that were more suitable for clinical and experimental applications. The heme is the prosthetic group of Hb. Results from MALDI-TOF MS showed that the peak intensity of heme (m/z = 616.4) was also high in these samples with high Hb levels, suggesting the contents of heme in discs could directly reflect Hb levels (Fig. 2a). Figure 2b indicated that the heme and its isotopes had evaluated levels in degenerative discs compared to the normal control. Then, the intensity of heme-related peaks in 10 cases of degenerative discs and 6 cases of normal discs was further detected. Visualized scatter plots indicated significant differences in the total intensity (Fig. 2c) and average intensity (Fig. 2d) between these two groups. It showed that the heme was specifically increased in degenerative discs, which was also consistent with the analysis results of Hb, and once again revealed pathological features of vasculogenesis in degenerative discs. Moreover, ROC curves were performed to assess diagnostic value of heme in degenerative discs. In this model, all data

had good diagnostic accuracy, and one data predicted degeneration with sensitivity of 80% and specificity of 85.7% (Fig. 2e).

Hb and heme levels are positively correlated with Pfirrmann classification of disc degeneration

Clinically, disc degeneration is graded according to the alteration in T2WI signal of parasagittal MRI images of dysfunctional segments combined with Pfirrmann classification. As shown in Fig. 3a, the nucleus pulposus with Pfirrmann's grade 1 was uniform and well demarcated with the annulus, while the nucleus and annulus with Pfirrmann's grade 3 or 4 were poorly defined margins. The signal of degenerative discs with Pfirrmann's grade 3 or 4 was reduced and became gray-black in MRI images. In order to verify the correlation between the vasculogenesis and the clinicopathology in degenerative discs, tissues were tested using MALDI-TOF MS and comparisons were performed with representative MRI images before surgery. The intensity of Hb-related peaks in degenerative discs with Pfirrmann's grade 3 or 4 was significantly higher than that in discs with Pfirrmann's grade 1 (Fig. 3b). Hb was increased as a result of vasculogenesis, accordingly, vasculogenesis might be closely associated with LDH progression. Furthermore, a similar result was observed for heme analyzed by MALDI-TOF MS. Results from Fig. 3c revealed that peak intensity of heme in degenerative discs with Pfirrmann's grade 3 or 4 was significantly higher than that in discs with Pfirrmann's grade 1.

High abundances of Hb and heme induce ferroptosis in degenerative tissues

The avascular tissue discs might be not responsible for initiating disc degeneration, but, secondary vasculogenesis could further promote the degeneration progression. As shown in Fig. 4a, heme was formed by iron and porphyrin. The heme-iron in Hb was very stable because of the tight arrangement of molecule. But, the non-protein-bound heme was hydrophobic and could enter cell membranes easily. As a result, heme was degraded by HO-1 to yield free iron, which was able to enhance oxidative stress and induce ferroptosis in cells. Interestingly, MALDI-TOF MS results indicated the increase of Hb was accompanied by the formation of crosslinked Hb, a marker of precedent formation of ferrylHb, implying Hb was oxidized and heme-iron dissociated from the resultant ferrylHb (Fig. 4b). It was tempting to speculate that the released iron could further induce oxidative stress and ferroptosis in degenerative discs. To test this, WB was performed to analyze the levels of Hb α, Hb β, the endothelial marker CD31, HO-1, and the ferroptosis suppressor GPX4 in 5 cases of degenerative discs and 3 cases of normal discs. As shown in Fig. 4c, consistent with MALDI-TOF MS results, degenerative tissues had increased Hb α and Hb β protein levels as compared with the normal group. The CD31 was significantly over-expressed in two cases of degenerative tissues, while it was almost not expressed in the control group, which also verified the reliability of above results based on MALDI-TOF MS. Meanwhile, HO-1, a response for heme catabolism, was highly expressed in the two degraded tissues with high CD31 levels, which could induce reactive oxygen species (ROS) production and ferroprosis in degenerative discs (Fig. 4c). Moreover, IHC results shown that although the cell number was significantly decreased and histological structure was

lost, we still observed the specific expression of HO-1 and GPX4 proteins in degenerative discs compared to normal discs (Fig. 4d).

Finally, ROS related metabolites in degenerative and normal discs were identified by high-resolution MALDI-TOF MS. As shown in Fig. 4f, normal discs were closed avascular tissues, in which the number and the intensity of detectable metabolites were significantly less than that of degenerative discs. Through accuracy mass measurements, a total of 28 endogenous metabolites were identified in degenerative discs and all these metabolites were used as ferroptosis-related metabolic pathways involving in glutathione metabolism, glycine metablism, arachidonic acid (AA) metabolism, sphinganine metabolism, polyunsaturated fatty acid (PUFA) metabolism, and tricarboxylic acid (TCA) cycle. These results suggested a state of high oxidative stress in the interior of degenerative discs, which would further accelerate the disc degeneration.

Heme induces ferroptosis in human nucleus pulposus cells

In order to confirm the effects of heme-iron on discs, the cell viability was tested after treating with differing concentration of heme in HNPCs, and erastin and FAC were used as ferroptosis positive controls. As seen in Fig. 5a-c, the inhibitory effects of heme, FAC, and erastin on cell viability were dose-dependent in HNPCs. As shown in Fig. 5d-f, GPX4 protein levels were also found decreased after treating with heme, FAC, and erastin in HNPCs, indicating all three could induce intracellular ROS and cell death. The anti-apoptotic molecular Bcl-2 and pro-apoptotic molecular Bax marked the occurrence of cell apoptosis. Results from Fig. 5d also showed that Bcl-2 protein levels were down-regulated when treated with 20 μg/ml heme in HNPCs, whereas Bax levels were increased when treated with 10 μg/ml heme in HNPCs. Based on the results of Fig. 5a, we could deduced that heme-induced ferroptosis occurred before apoptosis in HNPCs. Furthermore, in HNPCs, ROS related metabolic pathways in HNPCs were identified by high-resolution MALDI-TOF MS after heme, FAC, or erastin treatment (Fig. 5g). Similar to the analysis results at tissue levels, the number and the intensity of detectable metabolites were significantly increased after heme and FAC treatment in HNPCs. These differentially expressed metabolites are involved in glutathione metabolism, glycine metablism, AA metabolism, sphinganine metabolism, PUFA metabolism, and TCA cycle. The number of detectable metabolites in the erastin group was also decreased compared to heme and FAC groups. The reason was that the inhibitory effects of erastin on HNPCs were higher, and high death rates among cells weakened the MS signals (Fig. 5g).

Although heme induced a decrease in cell viability, this event could be significantly rescued by cotreatment with DFO, demonstrating heme-induced cell death was iron-dependent (Fig. 5h). Also, our results confirmed that heme-mediated inhibition of GPX4 protein could be rescued by DFO in HNPCs (Fig. 5h).

Heme-induced ferroptosis might be mediated by Notch pathway in HNPCs

Since numberous studies have reported that inhibition of Notch signaling pathway were involved in disc degeneration (Xiong et al. 2020; Long et al. 2019), we then investigated the related protein and mRNA changes in Notch signals after heme treatment. As depicted in Fig. 6a-b, there were significant changes in protein and mRNA levels of Notch1, Notch2, Jag1, Jag2, Hes1, Hes2, and Hey1 after heme treatment in HNPCs. Notably, we also found heme-induced inhibition of Notch-related molecules could be effectively rescued by DFO cotreatment. These results suggest that disc degeneration induced by heme-iron might be associated with the Notch signaling pathway.

Discussion

Although the accompanying vasculogenesis in the progression of disc degeneration had been observed a long time ago, traditional methods cannot accurately define the histopathological changes in degenerative discs. MALDI-TOF MS can quickly monitor the m/z of moleculars and provide mass information. It does not require chemical reagents to react with specific molecules in samples, thereby avoiding false positive or false negative results (van Smaalen et al. 2019; Grand et al. 2014). In this study, MALDI-TOF MS was combined with a high-mass detector which would not induce saturate effects in the presence of complex mixture over a broad mass range. Meanwhile, Our result was believed to be not affected by blood contamination because all samples were washed before extraction and prepared with a standard assay. Moreover, noticeable was that Hb polymers were detected in degenerative discs using our high-mass detector, marking the formation of ferrylHb (oxidized Hb), which make heme-iron dissociated from ferrylHb[11]. Then the release of iron further leads to endogenous oxidative stress and ultimately to cytotoxicity (Sardar Pasha et al. 2021; Gbotosho et al. 2020). Results from MALDI-TOF MS demonstrated that both Hb and heme contents were positively correlated with Pfirrmann classification of disc degeneration. Based on this, we proposed that heme-induced ferroptosis involved in the process of disc degeneration.

Ferroptosis is mainly induced by the inactivation of membrane lipid repair enzyme-GPX4, which caused the accumulation of ROS on membrane lipids, and this process is iron depend (Forcina et al. 2019). HO-1, a key enzyme for heme-iron degradation, also plays the dual role of pro-oxidation and anti-oxidation. Studies have shown that HO-1 could not only enhance the chemotherapeutic sensitivity of cancer cells, but also induce cell death by regulating iron homeostasis (Waza et al. 2018). HO-1 were also highly expressed in human smooth muscle cells and macrophages of atherosclerotic lesions[11]. As expected, in this study, elevated levels of GPX4 and HO-1 were found in degenerative tissues compare with normal discs, indicating a state of high oxidative stress in the interior of degenerative discs.

Erastin can inhibit the cystine-glutamate transporter on the membranes and reduce the cystine uptake by cells, which hinders the synthesis of glutathione, the substrate of GPX4. Finally, ferroptosis is usually produced as a result of lipid ROS generation (Forcina et al. 2019). Our results showed heme induced the same cell death effects as the erastin and FAC. Significantly, heme-induced ferroptosis could be rescued by DFO in HNPCs, and this results might provide some ideas for the non-surgical intervention of LDH,

perhaps clinically, it was possible to delay the disc degeneration by inhibiting vasculogenesis or regulating iron metabolism in LDH patients.

Notch signals is involved in multiple cellular processes, including cell survive, differentiation, apoptosis, and regeneration (Siebel et al. 2017). Besides, Notch signals is crucial for chondrogenesis and cartilage development (Hardingham et al. 2006). Recent studies have reported Notch could promote proliferation and inhibit apoptosis in cells derived from degenerative discs (Long et al. 2019). The expression levels of Notch also increased in the disc cells of patients with different Modic changes (Xiong et al. 2020). Our studies suggests disc degeneration induced by heme-iron is mediated by Notch signaling pathway, which will be a promising target to redirect degeneration for LDH therapy. This mechanism was presented in Fig. 7.

Conclusions

Our findings suggest that high levels of Hb and heme can be used to mark neovasculogenesis in degenerative discs, which further promote disc degeneration through heme-iron dependent cell death. These results are useful for in-depth study of degenerative pathology, and will provide new ideas for conservative treatment of LDH patients, such as intervention in vasculogenesis.

Abbreviations

MALDI-TOF MS
Matrix-assisted laser desorption/ionization time-of-flight mass spectrometry
Hb
Hemoglobin
GPX4
Glutathione peroxidase 4
AA
Glutathione, arachidonic acid
PUFA
Sphinganine, polyunsaturated fatty acid
TCA
Tricarboxylic acid cycle
LDH
Lumbar disc herniation
RBCs
Red blood cells
HNPCs
Human primary nucleus pulposus cells
DFO
Deferoxamine mesylate salt

FAC
Ferric ammonium citrate
PMSF
Phenylmethylsulfonyl fluoride
Hmdb
Human metabolome database
HO-1
Heme oxygenase-1
OD
Optical density
PCA
Principal component analysis
ROC
Receiver operating curve (ROC)
ROS
Reactive oxygen species (ROS)

Declarations

Ethics approval and consent to participate

All patients accepted informed consent before enrollment. The study was conducted in accordance with the Declaration of Helsinki, and the protocol was approved by the Medical Ethics Committee, Shanghai Changzheng Hospital.

Consent for publication

Not applicable.

Availability of data and materials

All the data are included within the main article.

Competing interests

The authors have declared that no competing interest exists.

Funding

This work was funded by National Natural Science Foundation of China (No. 21672250, No. 81871828, and No. 81702141) and Science and Technology Innovation Action Plan of Shanghai (No.19142201400).

Authors' contributions

The manuscript was written through contributions of all authors. All authors read and approved the final manuscript.

Acknowledgements

Not applicable.

References

1. Yao M, et al. A comparison between the low back pain scales for patients with lumbar disc herniation: validity, reliability, and responsiveness. Health Quality of Life Outcomes. 2020;18:175. doi:10.1186/s12955-020-01403-2.
2. Qiu C, et al. Differential proteomic analysis of fetal and geriatric lumbar nucleus pulposus: immunoinflammation and age-related intervertebral disc degeneration. BMC Musculoskelet Disord. 2020;21:339. doi:10.1186/s12891-020-03329-8.
3. Doraisamy R, et al. Genetic Risk factors for Lumbar Disc Disease. Ann Med. 2002;34:42–7. doi:10.1080/078538902317338634.
4. Petra C, Karin WK. MicroRNAs in Intervertebral Disc Degeneration, Apoptosis, Inflammation, and Mechanobiology. Int J Mol Sci. 2020;21:3601. doi:10.3390/ijms21103601.
5. Arai Y, et al. Immunohistological study of intervertebral disc herniation of lumbar spine. Journal of Orthopaedic Science. 2000;5:229–31. doi:10.1007/s007760050156.
6. Xiao ZF, et al. Mechanics and Biology Interact in Intervertebral Disc Degeneration: A Novel Composite Mouse Model. Calcif Tissue Int. 2020;106:401–14. doi:10.1007/s00223-019-00644-8.
7. Yasuma T, Aral K, Yamauchi Y. The histology of lumbar intervertebral disc herniation. The significance of small blood vessels in the extruded tissue. Spine. 1993;18:1761–5. doi:10.1097/00007632-199310000-00008.
8. Nagy E, et al. Red Cells, Hemoglobin, Heme, Iron and Atherogenesis. Arterioscler Thromb Vasc Biol. 2010;30:1347–53. doi:10.1161/ATVBAHA.110.206433.
9. Jeney V, et al. Pro-oxidant and cytotoxic effects of circulating heme. Blood. 2002;100:879–87. doi:10.1182/blood.v100.3.879.
10. Hower V, et al. A General Map of Iron Metabolism and Tissue-specific. Mol Biosyst. 2009;5:422–43. doi:10.1039/b816714c.
11. Yin L, et al. Rev-erbalpha: a heme sensor that coordinates metabolic and circadian pathways. Science. 2007;318:1786–9. doi:10.1126/science.1150179.
12. Dixon SJ, et al. Ferroptosis: An Iron-Dependent Form of Nonapoptotic Cell Death. Cell. 2012;149:1060–72. doi:10.1016/j.cell.2012.03.042.
13. Buss JL, et al. Iron chelators in cancer chemotherapy. Curr Top Med Chem. 2004;4:1623–35. doi:10.2174/1568026043387269.

14. Zhang P, et al. Ferroptosis was more initial in cell death caused by iron overload and its underlying mechanism in Parkinson's disease. Free Radic Biol Med. 2020;152:227–34. doi:10.1016/j.freeradbiomed.2020.03.015.
15. Wang H, et al. Improvement and extension of the application scope for matrix-assisted laser desorption/ionization mass spectrometric analysis-oriented N-alkylpyridinium isotope quaternization. Anal Chim Acta. 2011;70:100–6. doi:10.1016/j.aca.2011.09.019.
16. Wieczorek M, et al. Immunoglobulin G Subclass-Specific Glycosylation Changes in Primary Epithelial Ovarian Cancer. Front Immunol. 2020;11:654. doi:10.3389/fimmu.2020.00654.
17. van Smaalen TC, et al. Rapid Identification of Ischemic Injury in Renal Tissue by Mass-Spectrometry Imaging. Anal Chem. 2019;91:3575–81. doi:10.1021/acs.analchem.8b05521.
18. Grant RP, Hoofnagle AN. From lost in translation to paradise found enabling protein biomarker method transfer by mass spectrometry. Clin Chem. 2014;60:941–4. doi:10.1373/clinchem.2014.224840.
19. Orellano LAA, et al. Implant-induced inflammatory angiogenesis is up-regulated in obese mice. Microvasc Res. 2020;131:104014. doi:10.1016/j.mvr.2020.104014.
20. Xiong ZK, et al. Correlation between the HIF-1α/Notch signaling pathway and Modic changes in nucleus pulposus cells isolated from patients with low back pain. BMC Musculoskelet Disord. 2020;21:500–7. doi:10.1186/s12891-020-03505-w.
21. Long J, et al. JAG2/Notch2 inhibits intervertebral disc degeneration by modulating cell proliferation, apoptosis, and extracellular matrix. Arthritis Research Therapy. 2019;21:213–26. doi:10.1186/s13075-019-1990-z.
22. Sardar Pasha SPB, et al. Retinal Phenotyping of Ferrochelatase Mutant Mice Reveals Protoporphyrin Accumulation and Reduced Neovascular Response. Invest Ophthalmol Vis Sci. 2021;62:36. doi:10.1167/iovs.62.2.36.
23. Gbotosho OT, Kapetanaki MG, Kato GJ. The Worst Things in Life are Free: The Role of Free Heme in Sickle Cell Disease. Front Immunol. 2020;11:561917. doi:10.3389/fimmu.2020.561917.
24. Forcina GC, Dixon SJ. GPX4 at the Crossroads of Lipid Homeostasis and Ferroptosis. Proteomics. 2019;19:e1800311, oi: 10.1002/pmic.201800311.
25. Waza AA, et al. A review on heme oxygenase-1 induction: is it a necessary evil. Inflamm Res. 2018;67:579–88. doi:10.1007/s00011-018-1151-x.
26. Siebel C, Lendahl U. Notch Signaling in Development, Tissue Homeostasis, and Disease. Physiol Rev. 2017;97:1235–94. doi:10.1152/physrev.00005.2017.
27. Hardingham TE, Oldershaw RA, Tew SR. Cartilage, SOX9 and Notch signals in chondrogenesis. J Anat. 2006;209:469–80. doi:10.1111/j.1469-7580.2006.00630.x.

Figures

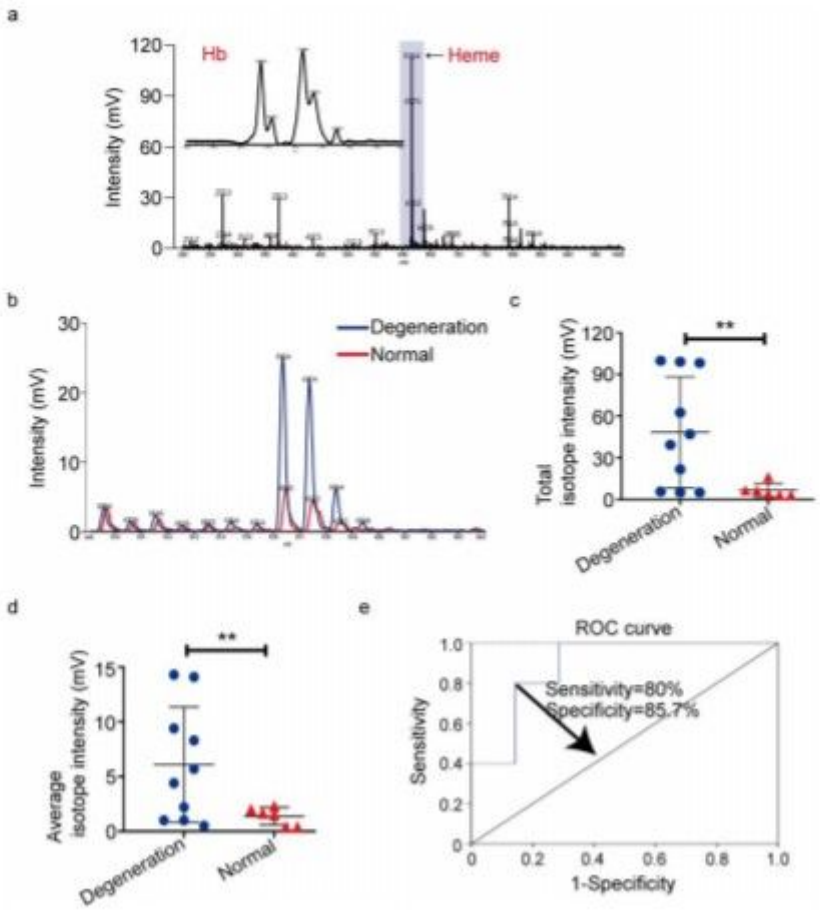

Figure 2

Specific increase in heme content in degenerative discs analyzed by MALDI-TOF MS. (a) MS spectra of total protein lysates at low-mass range. (b) The spectra of tissue lysates from degenerative discs and normal discs at low-mass range. (c-d) The total intensity (c) and average intensity (d) of the heme and its isotope peaks in 10 cases of degenerative discs and 6 cases of normal discs, Data were represented with GraphPad Prism 5.02. **P<0.01. (e) The ROC curve analysis of heme peaks in 10 cases of degenerative discs and 6 cases of normal discs.

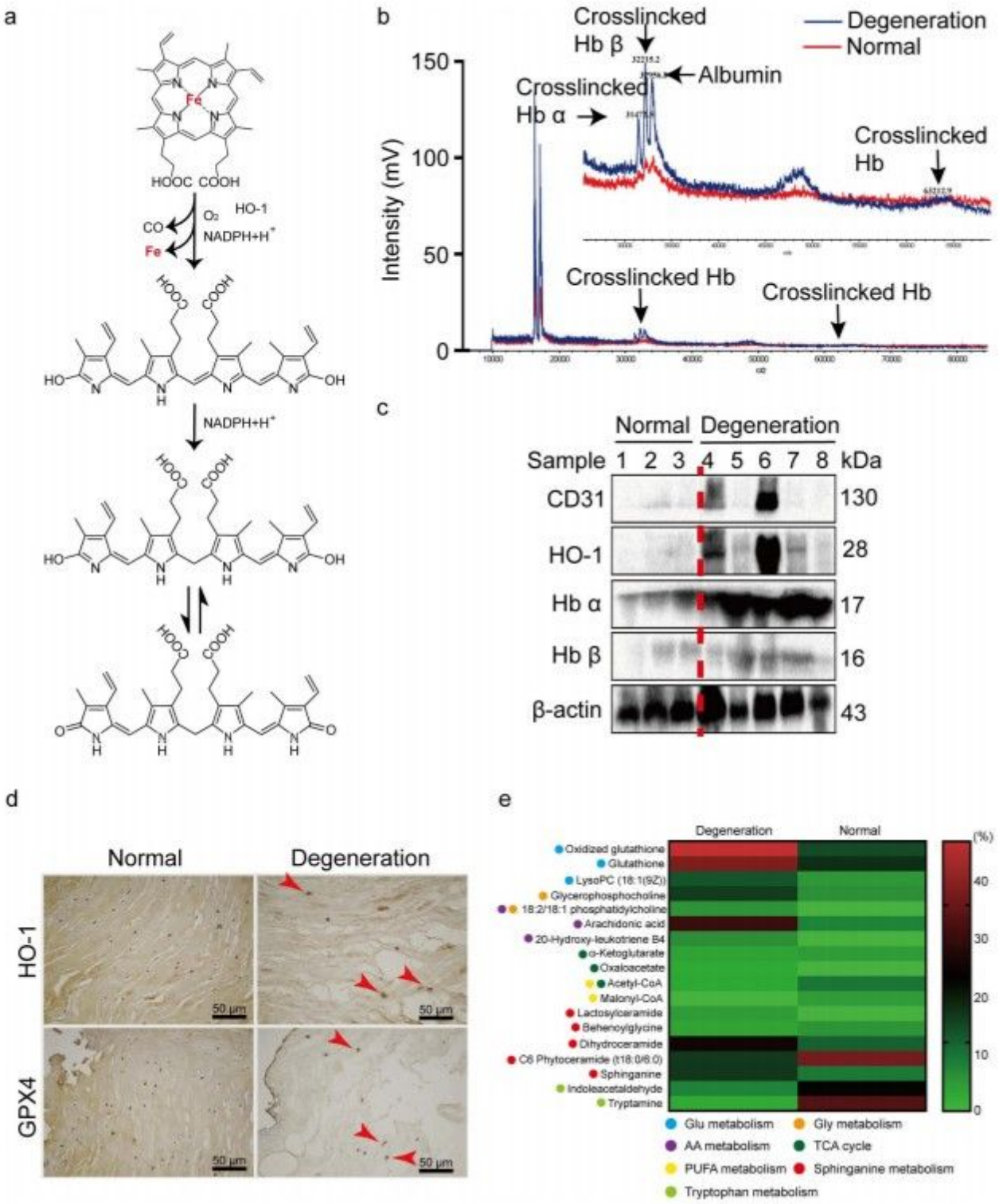

Figure 4

High abundances of Hb and heme induce ferroptosis in degenerative tissues. (a) Heme degeneration catalyzed by HO-1. (b) Hb polymers were detected by MALDI-TOF MS in degenerative discs. (c) The protein levels of CD31, HO-1, Hb α, and Hb β in 5 cases of degenerative discs and 3 cases of normal discs. (d) HO-1 and GPX4 protein levels in degenerative and normal tissues as determined by immunohistochemical analysis. The representative IHC images were taken at a magnification of 200×.

(e) Identification results of ROS and ferroptosis-related metabolites in degenerative and normal discs using high-resolution MALDI-TOF MS.

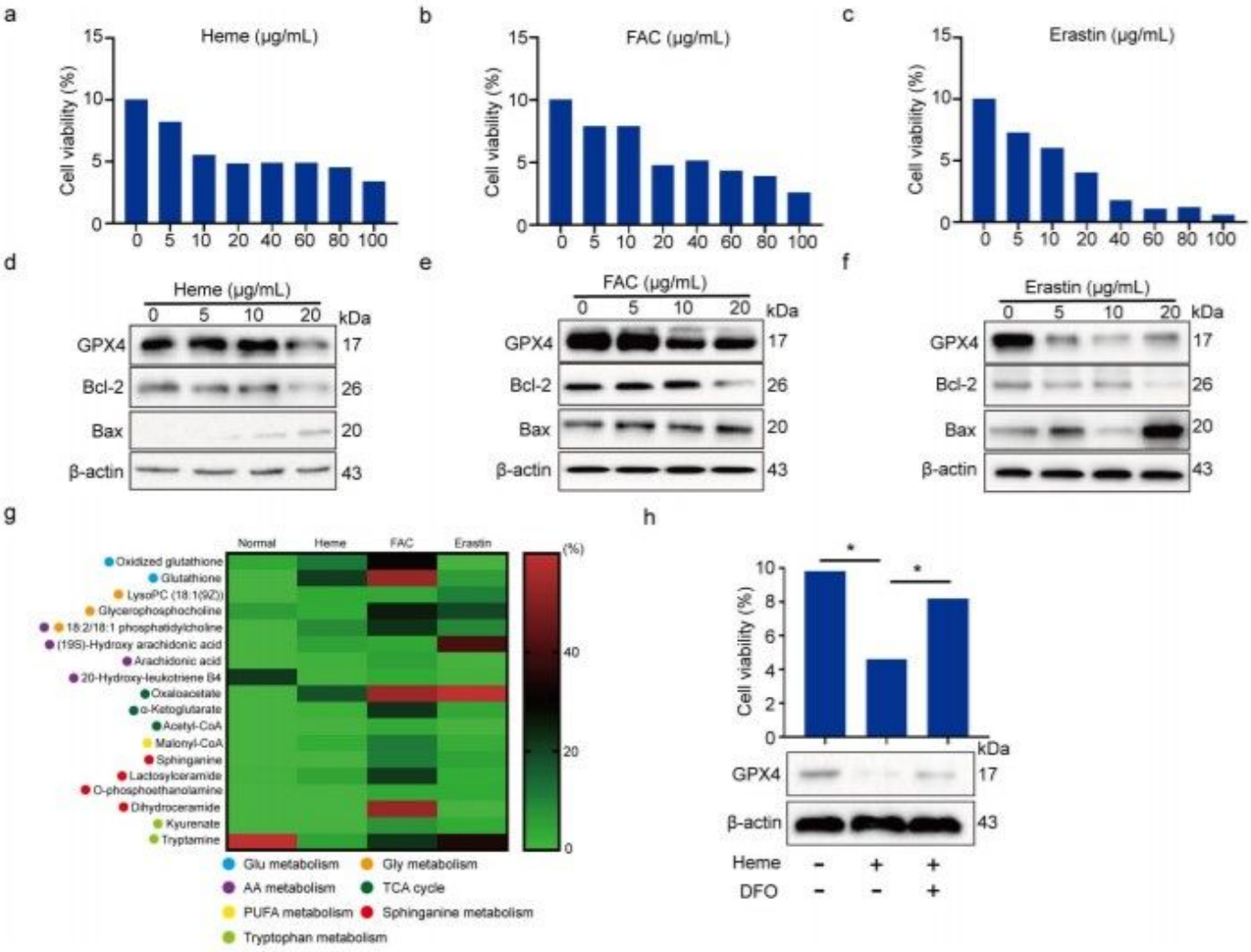

Figure 5

Heme induces ferroptosis in human nucleus pulposus cells. (a-c) Cell viabilities were measured by CCK-8 in HNPCs treated with heme (a), FAC (b), and erastin (c) at the concentrations of 0, 5, 10 ,20, 40, 60, 80, and 100 μg/mL for 24 h. Data was represented with GraphPad Prism 5.02. (d-f) The protein levels of GPX4, Bcl-2, and Bax in HNPCs treated with heme (d), FAC (e), and erastin (f) at the concentrations of 0, 5, 10, and 20 μg/mL for 24 h. (g) Cell viabilities were measured by CCK-8 in HNPCs after 20 μg/mL heme treatment for 24 h with or without 30 μg/mL DFO pretreatment for 1h (upper), and the protein levels of GPX4 in HNPCs after 20 μg/mL heme treatment for 24 h with or without 30 μg/mL DFO pretreatment for 1 h (lower). (H) Identification results of ROS and ferroptosis-related metabolites in HNPCs after treating with 20 μg/mL heme, 20 μg/mL FAC, and 10 μg/mL Erastin for 24 h using high-resolution MALDI-TOF MS.